

A COMPARISON OF TWO MODELS FOR THE SEPARATION OF DIRECT AND DIFFUSE IRRADIANCE IN PLANE OF ARRAY

Dorian Esteban Guzman Razo, Sven Killinger, Björn Müller, Christof Wittwer
 Fraunhofer ISE, Fraunhofer Institute for Solar Energy Systems ISE
 Heidenhofstraße 2, 79110 Freiburg, Germany
 Tel.: 0761 4588 5826, email: dorian.esteban.guzman.razo@ise.fraunhofer.de

ABSTRACT: For advanced automated operational monitoring of Photovoltaic (PV) systems, e.g. in order to distinguish losses due to self-shading from malfunctions, direct and diffuse irradiance at the module plane (plane of array, POA) are required separately. However, in practice, usually only measured values of global POA irradiance (G_{POA}) are recorded on site. There is thus a need for a model to divide G_{POA} into its direct (I_{POA}) and diffuse components (D_{POA}). This paper compares and evaluates two models recently developed that perform such separation. The aim of this work is to show the advantages and disadvantages that these two models offer and how they differ from each other. In order to compare and evaluate them, two different POA data sets were used. The first data set is generated using SolarGIS satellite-based data for 16 different locations across Germany. The second data set contains on-site measured D_{POA} and G_{POA} data from a PV power plant located in south-west Germany. Results from both models show good matching with satellite-based data from the 16 different locations.

Keywords: Modelling, Photovoltaic, PV System, Solar irradiance models, Decomposition in plane of array

1 INTRODUCTION

Due to the increase of the global PV installed capacity around the world, the challenges for an accurate simulation of the overall system's behavior under outdoor conditions have increased as well. It is known that the PV system's energy output depends to a large extent on G_{POA} and on its components: I_{POA} and D_{POA} .

Models for decomposing global horizontal solar irradiance into its direct and diffuse components have been developed and evaluated for decades, e.g. [1–4]. These models are part of many calculation methods for yield forecasting and well validated for many regions of the Earth. However, to the knowledge of the authors, similar models for irradiance decomposition in POA do not exist up to now.

In practical terms, measurements of G_{POA} are commonly available within medium and large-scale PV installations which provide just enough data for the calculation of plant's key performance indicators (KPIs) such as Performance Ratio (PR) and Availability. Yet, if a more detailed and accurate PV system modelling is required in order to now-cast and forecast power production, this information is not sufficient and a decomposition of G_{POA} into I_{POA} and D_{POA} is necessary.

1.1 Background and literature review

In early 2019, two different models for G_{POA} into I_{POA} and D_{POA} separation have been introduced: [5,6]. Both empirical approaches are similarly inspired by the concept of the classic diffuse (K_d) and clearness index (K_t) fraction introduced by [7], described by Equation (1) and Equation (2).

$$K_t = \frac{GHI}{G_{EXT}} \quad (1)$$

$$K_d = \frac{DIF}{GHI} \quad (2)$$

Where GHI is the global horizontal irradiance, G_{EXT} is the extra-terrestrial irradiance and DIF is the diffuse horizontal irradiance.

For convenience in the following sections of this work, the model in [5] will be referred as Mod1, the model in [6] approach A will be referred as Mod2A and the model in [6] approach B will be referred as Mod2B.

In the models compared here, both indexes are defined on plane of array described by Equation (3) and Equation (4).

$$K_{t,POA} = \frac{G_{POA}}{G_{EXT,POA}} \quad (3)$$

$$K_{d,POA} = \frac{D_{POA}}{G_{POA}} \quad (4)$$

1.2 Outline and objective

The aim of this work is to compare both G_{POA} separation models using two datasets. The first one consists of GHI and DIF satellite-derived data provided by SolarGIS, combined with a transposition model ([8]) and the second dataset consists of G_{POA} and D_{POA} measured data.

The paper is structured in the following way: Section 2 contains the steps followed in order to compare the two models and describes, as well, the data used within this work. In Section 3, results from the comparison of the two models are provided. And finally, a brief summary of this work and avenues for future research are presented in Section 4.

1.3 Models description

Mod1, on the one hand, is mainly based on the two indexes above mentioned (Equations (3) and (4)). Similar to the already known models for the horizontal plane, in this case, however, the diffuse fraction in plane of array ($K_{d,POA}$) is defined as a function of the Clearness Index ($K_{t,POA}$) and angle of incidence (AOI, in radians); see Equation (5).

$$K_{d,POA} = f(K_{t,POA}, AOI) \quad (5)$$

Mod2A and Mod2B, on the other hand, are described in a general way by the diffuse fraction in plane of array $K_{d,POA}$ as a piece-wise function of $K_{t,POA}$, the sun's zenith angle (θ_z), the PV system's azimuth angle (α) and the PV system's tilt angle (β), with similar set of limits for $K_{d,POA}$ to the model proposed by [9]. See Equation (6).

$$K_{d,POA} = f(K_{t,POA}, \theta_z, \alpha, \beta) \quad (6)$$

Once $K_{d,POA}$ has been calculated, it is possible to obtain D_{POA} using Equation (4), and thus to calculate I_{POA} with Equation (7).

$$G_{POA} = D_{POA} + I_{POA} \quad (7)$$

This work is focused on D_{POA} calculation from G_{POA} ; therefore, I_{POA} calculations are not presented.

In order to calculate $K_{d,POA}$, Mod1 offers a straightforward third-degree-like equation defined as follows:

$$\begin{aligned} K_{d,POA}(K_{t,POA}, AOI) = & C_1 K_{t,POA} + C_2 AOI \\ & + C_3 (K_{t,POA})^2 + C_4 K_{t,POA} AOI + C_5 (AOI)^2 \\ & + C_6 (K_{t,POA})^3 + C_7 (K_{t,POA})^2 AOI \\ & + C_8 K_{t,POA} (AOI)^2 + C_9 (AOI)^3 + C_{10} \end{aligned} \quad (8)$$

All the constants are already optimized and defined for any given case of $K_{d,POA}$. Table I shows the constants' values presented in Equation (8).

Table I: Optimized values of Mod1 model's constants. Values for C_1 to C_{10} to calculate any possible value of $K_{d,POA}$.

| Constant | Value |
|----------|---------|
| C_1 | 1.3052 |
| C_2 | 0.9739 |
| C_3 | -4.6871 |
| C_4 | -1.8813 |
| C_5 | -1.1749 |
| C_6 | 2.7340 |
| C_7 | 1.18 |
| C_8 | 0.7127 |
| C_9 | 0.444 |
| C_{10} | 0.7361 |

Mod2A and Mod2B propose a general equation for $K_{d,POA}$ calculation depending on the $K_{t,POA}$ value, considering a similar set of limits as the method proposed by [9]. This means that $K_{d,POA}$ can be calculated as follows:

$$K_{d,POA} = a_i + b_i * K_{t,POA} + c_i * \cos \theta_z \quad (9)$$

Where the sub-index i , is chosen depending on the $K_{t,POA}$ value, as mentioned before, according to the limits shown in Table II.

Table II: Definition of sub-index i depending on $K_{t,POA}$ values for Equation (9). When the $K_{t,POA}$ value is between 0 and 0.3, inclusive, i is equal to 1. When $K_{t,POA}$ value is higher than 0.3 but lower than 0.78, i is equal to 2. When $K_{t,POA}$ value is 0.78 or higher, i is equal to 3.

| Limits | Index i |
|------------|-----------|
| [0,0.3] | 1 |
| (0.3,0.78) | 2 |
| [0.78, +∞) | 3 |

Mod2A and Mod2B also propose two different approaches in order to calculate the coefficients $a_i, b_i, c_i (i = 1,2,3)$, both as a function of β and α ($f_i(\alpha, \beta)$), as Equation (10), for approach A, and Equation (11), for approach B, indicate.

$$f_i(\alpha, \beta)_A = \frac{\beta(\alpha)}{90^\circ} * (\theta_l(\alpha) - m_{3,l}) + \phi_l(\beta) \quad (10)$$

$$f_i(\alpha, \beta)_B = \theta_l(\alpha) + \phi_l(\beta) - m_{3,l} \quad (11)$$

Where the sub-index l is defined by the previous definition of $a_i, b_i, c_i (i = 1,2,3)$. Equations (12) and (13) define functions $\phi_l(\beta)$ and $\theta_l(\alpha)$, respectively.

$$\phi_l(\beta) = d_{1,l} * \beta^2 + d_{2,l} * \beta + d_{3,l} \quad (12)$$

$$\theta_l(\alpha) = m_{1,l} * \alpha^2 + m_{2,l} * \alpha + m_{3,l} \quad (13)$$

In order to calculate coefficients $a_i, b_i, c_i (i = 1,2,3)$ from Equation (9) with either approach A or B, first coefficients $d_{i,l}$ and $m_{i,l} (i = 1,2,3)$ have to be defined for $l \in \{1,2, \dots, 9\}$. Table III offers the optimum values for those coefficients. $K_{d,POA}$ values higher than 1 are set to 1 and $K_{d,POA}$ lower than 0 are set to 0.

Table III: Optimized values for Mod2A and Mod2B constants. Approach A and B coefficients $d_{i,l}$ and $m_{i,l} (i = 1,2,3)$, needed to calculate any possible value of $a_i, b_i, c_i (i = 1,2,3)$, defined by Equations (10), (11), (12) and (13).

| l | $f_i(\alpha, \beta)$ | $m_{1,l}$ | $m_{2,l}$ | $m_{3,l}$ |
|-----|----------------------|-----------|-----------|-----------|
| 1 | a_1 | -1.79E-5 | -0.0001 | 0.7635 |
| 2 | b_1 | -4.5E-5 | -0.0007 | -0.5968 |
| 3 | c_1 | 4.27E-5 | 0 | 0.3956 |
| 4 | a_2 | -2.72E-5 | 0.0002 | 0.7784 |
| 5 | b_2 | 1.49E-5 | -0.0013 | -1.4297 |
| 6 | c_2 | 3.17E-5 | 0.0007 | 0.7694 |
| 7 | a_3 | -3.01E-5 | -0.0002 | 0.2265 |
| 8 | b_3 | 0.68E-5 | 0.0008 | 0.5090 |
| 9 | c_3 | 3.72E-5 | -0.0007 | -0.4251 |
| l | $f_i(\alpha, \beta)$ | $d_{1,l}$ | $d_{2,l}$ | $d_{3,l}$ |
| 1 | a_1 | 0 | -0.0021 | 0.9604 |
| 2 | b_1 | 5.21E-5 | -0.0111 | -0.0191 |
| 3 | c_1 | 0 | 0.0040 | 0.0367 |
| 4 | a_2 | 0 | -0.0069 | 1.3824 |
| 5 | b_2 | -11.15E-5 | 0.0149 | -1.8707 |
| 6 | c_2 | 6.55E-5 | -0.0003 | 0.2692 |
| 7 | a_3 | 2.57E-5 | 0.0008 | -0.0490 |
| 8 | b_3 | -9.19E-5 | 0.0075 | 0.5763 |
| 9 | c_3 | 8.76E-5 | -0.0104 | -0.1947 |

It is important to mention that, Mod2A and Mod2B define the PV system's azimuth angle (α) as 0° when is south oriented, as -90° for the east and as 90° for the west. Whereas in Mod1 south is defined as 180° , east as 90° and west as 270° .

2 METHODOLOGY AND DATA

Two different datasets were used for this work. The first dataset consists of satellite-derived data provided by SolarGIS for 16 real PV systems distributed throughout Germany (on site pyranometer measurements of G_{POA} are not available for these sites). This dataset offers data from January 1994 until February 2018 with 15 minutes

time resolution. The second dataset provides on-site G_{POA} and D_{POA} measured data from a SPN1 pyranometer installed in south-west Germany, including dates from 22/03/2011 until 24/09/2015 with 5 minutes time resolution. See Figure 1 and Table IV for details.

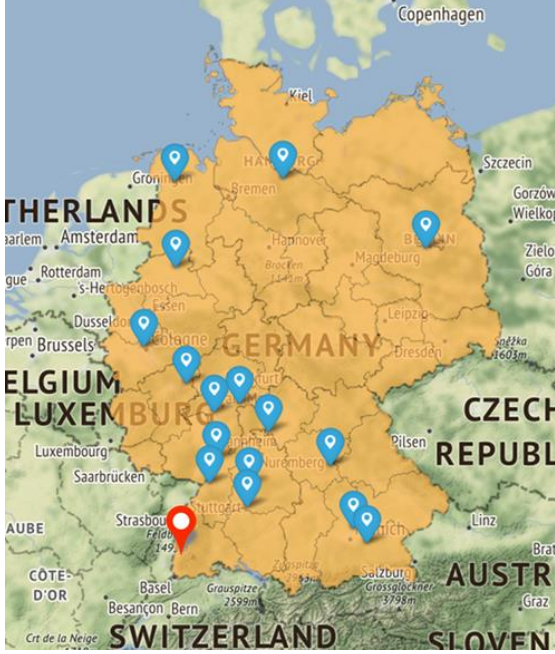


Figure 1: The 16 real PV systems and the PV system on-site measured data. The pointers in blue represent the geographical location of the synthetic data generated for this work. The red pointer represents the location of the SPN1 pyranometer measured data.

Table IV: Azimuth and Tilt angles for each one of the 16 real PV systems and the PV system on-site measured. Azimuth angles are defined based on the Mod1's standard. * On-site measurements.

| System ID | System Azimuth Angle [°] | System Tilt Angle [°] |
|-----------|--------------------------|-----------------------|
| 1 | 177 | 30 |
| 2 | 213 | 15 |
| 3 | 190 | 15 |
| 4 | 215 | 15 |
| 5 | 182 | 15 |
| 6 | 203 | 15 |
| 7 | 172 | 15 |
| 8 | 152 | 15 |
| 9 | 162 | 15 |
| 10 | 191 | 15 |
| 11 | 156 | 25 |
| 12 | 195 | 25 |
| 13 | 174 | 25 |
| 14 | 160 | 15 |
| 15 | 208 | 25 |
| 16 | 180 | 25 |
| 17* | 237.5 | 27 |

In order to generate D_{POA} data, SolarGIS data from System ID 1 to 16 have been simulated using Perez

transposition method proposed by [8], included in PVlib library ([10]). After that, $K_{t,POA}$ values from the 16 PV systems have been calculated based on Equation (3). Finally, based on Equations (8) and (9), $K_{d,POA}$ values have been also calculated for Mod1, Mod2A and Mod2B. Clearing for D_{POA} from Equation (4) allows one to compare the D_{POA} simulated with the D_{POA} resulted from the two models.

$K_{t,POA}$ values for system ID 17 have been calculated in a similar fashion, but in this case using on-site measurements and Equation (3). Afterwards, $K_{d,POA}$ values are calculated using the three models, based in Equations (8) and (9). Thus, clearing again for D_{POA} from Equation (4), including $K_{d,POA}$ values calculated previously, it is possible to compare the three models' resulting D_{POA} with D_{POA} on-site measured values.

The following filters have been applied for all the datasets, system ID 1 to 17: D_{POA} and G_{POA} values less than 10 W/m^2 (night-time) have been filtered out. Whereas, in order to exclude incorrect measurements that might lead to inappropriate conclusions, exclusively for System ID 17 additional filters have been included: Incomplete days and measurement errors (e.g. negative irradiance values) have been filtered out.

Finally, three common error indicators have been selected with the intention of having a better insight of the models' results: RSMD (Root Square Mean Deviation), nRSMD (Normalized Root Square Mean Deviation) and R^2 (coefficient of correlation).

RSMD and nRSMD are used to measure the differences between $K_{d,POA}$ predicted (E_i) and observed (O_i) samples or populations. These indicators are fundamentally an accuracy index where higher simulation deviations lead to higher RSMD and higher nRSMD percentage values (RSMD is normalized by the average of the observed points). These two indicators have been proposed before for this kind of experiments by [11] and are given by Equations (14) and (15) respectively.

$$RSMD = \sqrt{\frac{1}{N} \sum_{i=1}^N (E_i - O_i)^2} \quad (14)$$

$$nRSMD = \frac{1}{\bar{O}} \sqrt{\frac{1}{N} \sum_{i=1}^N (E_i - O_i)^2} \quad (15)$$

RSMD and NRSMD have been calculated by $K_{d,POA}$ of both, calculated (O_i) and simulated values (E_i) of Mod1, Mod2A and Mod2B.

In the case of R^2 , it is used to measure how well the model replicated the observed values, in other words, the correlation between the observed values and the predicted ones. This error measure has been included as well by [4], with the purpose of having an extra indicator of the model's performance and is given by the Equation (16).

$$R^2 = 1 - \frac{\sum_{i=1}^N (O_i - E_i)^2}{\sum_{i=1}^N (O_i - \bar{O})^2} \quad (16)$$

R^2 has been calculated with $K_{d,POA}$ simulated (or measured in the case of System ID 17) and $K_{d,POA}$ resulted values from Mod1, Mod2A and Mod2B.

In the three equations, (14), (15) and (16), the length of the population defines N, E is defined by the estimated value, O is the observed value and \bar{O} is the mean value over all data points.

3 RESULTS

As a first impression, Figure 2 and Figure 3 show the plotted $K_{d,POA}$ results from Mod1, Mod2A and Mod2B from System ID 9. The same plots have been generated for the other datasets with similar results. Therefore, the rest of the plots are not shown in this work.

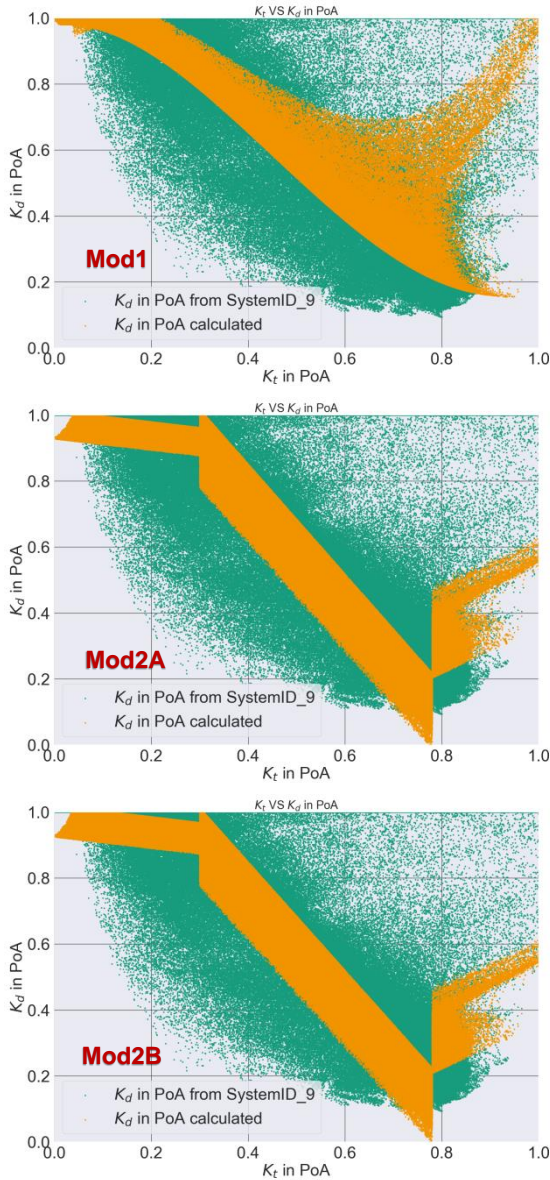


Figure 2: $K_{t,POA}$ versus $K_{d,POA}$ classic plots for the three models, System ID 9 dataset. The green dots represent the simulated SolarGIS data and orange dots represent the results from Mod1, Mod2A and Mod2B.

In Figure 2, at the top, results from $K_{t,POA}$ versus $K_{d,POA}$ Mod1 can be observed. In the middle of the figure, results from $K_{t,POA}$ versus $K_{d,POA}$ Mod2A can be observed. In the bottom of the figure, results from $K_{t,POA}$ versus $K_{d,POA}$ Mod2B can be observed.

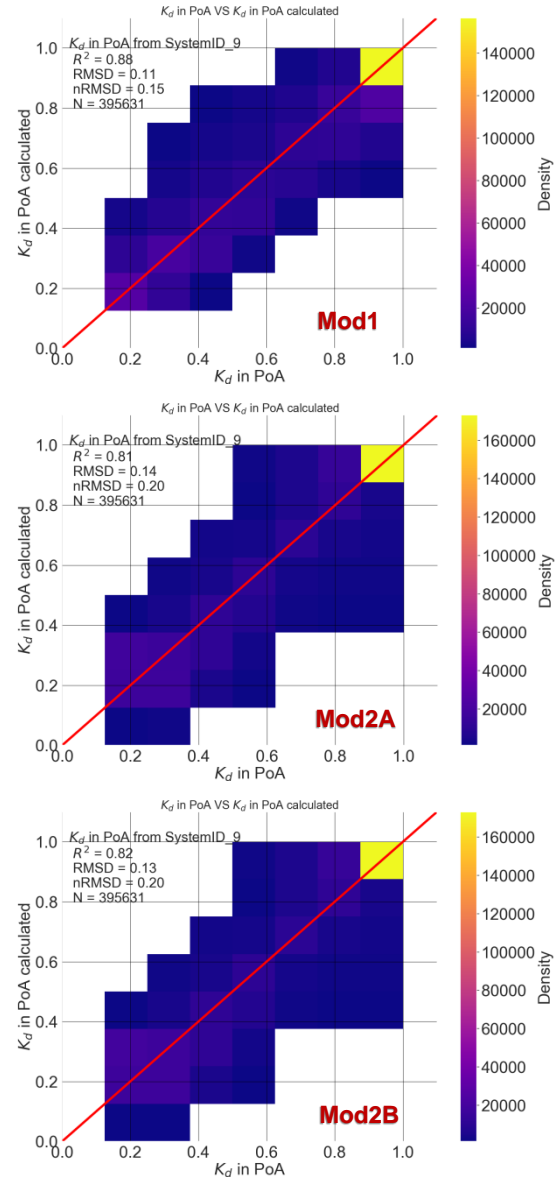


Figure 3: D_{POA} simulated values versus D_{POA} values calculated with the models from System ID 9 are represented by accumulative grid. Lower accumulation of values in a certain region is represented by dark-blue color while regions with 140,000+ values accumulated are colored in yellow.

The red line in Figure 3 shows when correlation equals to one. In the top of this figure, the plotted results of the Mod1 can be observed with 11 RMSD percentage points, 15 nRMSD percentage-normalized points and $0.88 R^2$. In the middle of this figure, the plotted results of Mod2A can be observed with 14 RMSD percentage points, 20 nRMSD percentage-normalized points and $0.81 R^2$. In the lower part of this figure, the plotted results of Mod2B can be observed with 13 RMSD percentage points, 20 nRMSD percentage-normalized points and $0.82 R^2$.

Furthermore, deviation metrics were evaluated separately for each one of the 16 systems and the measured system datasets. The condensed outcomes from the three models, Mod1, Mod2A and Mod2B are shown in Table V. System ID 17 has been excluded of the

average calculation due to the low quality of the data input.

Table V: Mod1, Mod2A and Mod2B results of the 16 systems and the measured system datasets. R^2 , nRMSD and RMSD average, minimum and maximum values can be observed.

* Not included in the calculation of average, minimum and maximum.

| System ID | Mod1 | | Mod2A | | Mod2B | |
|-----------|-------------|-------------|-------------|-------------|-------------|-------------|
| | R^2 | RMSD | R^2 | RMSD | R^2 | RMSD |
| 1 | 0.86 | 0.12 | 0.80 | 0.14 | 0.80 | 0.14 |
| 2 | 0.85 | 0.11 | 0.80 | 0.14 | 0.80 | 0.14 |
| 3 | 0.88 | 0.11 | 0.81 | 0.14 | 0.81 | 0.14 |
| 4 | 0.86 | 0.12 | 0.81 | 0.14 | 0.81 | 0.14 |
| 5 | 0.89 | 0.10 | 0.83 | 0.14 | 0.83 | 0.14 |
| 6 | 0.87 | 0.11 | 0.82 | 0.13 | 0.82 | 0.14 |
| 7 | 0.90 | 0.10 | 0.83 | 0.13 | 0.83 | 0.13 |
| 8 | 0.88 | 0.11 | 0.83 | 0.13 | 0.83 | 0.13 |
| 9 | 0.88 | 0.11 | 0.81 | 0.14 | 0.82 | 0.13 |
| 10 | 0.89 | 0.10 | 0.83 | 0.13 | 0.83 | 0.14 |
| 11 | 0.85 | 0.12 | 0.82 | 0.14 | 0.82 | 0.14 |
| 12 | 0.86 | 0.11 | 0.80 | 0.14 | 0.80 | 0.14 |
| 13 | 0.87 | 0.11 | 0.81 | 0.14 | 0.81 | 0.14 |
| 14 | 0.89 | 0.11 | 0.84 | 0.13 | 0.84 | 0.13 |
| 15 | 0.84 | 0.12 | 0.80 | 0.14 | 0.79 | 0.14 |
| 16 | 0.86 | 0.11 | 0.81 | 0.14 | 0.81 | 0.14 |
| Avg. | 0.87 | 0.11 | 0.82 | 0.14 | 0.82 | 0.14 |
| Max | 0.90 | 0.12 | 0.84 | 0.14 | 0.84 | 0.14 |
| Min | 0.84 | 0.10 | 0.80 | 0.13 | 0.79 | 0.13 |
| 17* | 0.75 | 0.17 | 0.60 | 0.22 | 0.57 | 0.22 |

| System ID | N | Mod1 | Mod2A | Mod2B |
|-----------|---------------|-------------|-------------|-------------|
| | | nRMSD | nRMSD | nRMSD |
| 1 | 386329 | 0.18 | 0.22 | 0.22 |
| 2 | 389808 | 0.16 | 0.20 | 0.21 |
| 3 | 398272 | 0.15 | 0.20 | 0.20 |
| 4 | 390095 | 0.17 | 0.21 | 0.21 |
| 5 | 401778 | 0.16 | 0.21 | 0.21 |
| 6 | 396173 | 0.16 | 0.20 | 0.20 |
| 7 | 400671 | 0.15 | 0.21 | 0.21 |
| 8 | 394811 | 0.16 | 0.20 | 0.20 |
| 9 | 395631 | 0.15 | 0.20 | 0.20 |
| 10 | 399891 | 0.15 | 0.21 | 0.21 |
| 11 | 385501 | 0.18 | 0.21 | 0.21 |
| 12 | 388206 | 0.17 | 0.21 | 0.21 |
| 13 | 390770 | 0.17 | 0.21 | 0.21 |
| 14 | 399051 | 0.16 | 0.21 | 0.20 |
| 15 | 380882 | 0.17 | 0.20 | 0.21 |
| 16 | 391001 | 0.17 | 0.21 | 0.21 |
| Avg. | 393054 | 0.16 | 0.21 | 0.21 |
| Max | 401778 | 0.18 | 0.22 | 0.22 |
| Min | 380882 | 0.15 | 0.20 | 0.20 |
| 17* | 183221 | 0.26 | 0.32 | 0.34 |

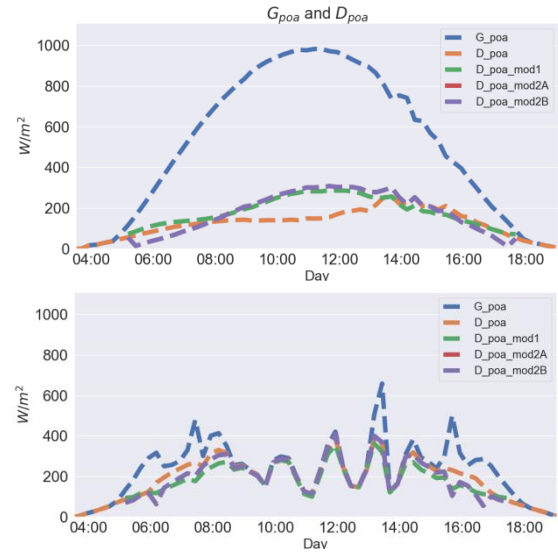


Figure 4: Two days of System ID 16, July 2016. The top plot shows a clear-sky-like day (19.07.2016) and the bottom plot shows a cloudy-like day (07.07.2016).

Table V shows the overall performance of the models and the results of R^2 , nRMSD and RMSD calculation can be observed. In the case of System ID 17, measured values are taken into consideration just as a proof of concept for these two models. In comparison, system 1 to 16 with system 17, the models seem to perform slightly worse. The reason may be attributed either to the fact that, at least for model 1, the parameters were fitted using satellite irradiance data, not measured data. Also, measurement uncertainties for system 17 may be quite high. Therefore, the results from System ID 17 are not to be considered as conclusive results.

Finally, Figure 4 shows two different days from July 2016. On the one hand, the first plot is a clear-sky-like day where also DPOA simulated data and results from Mod1, Mod2A and Mod2B can be observed. It is notable that both models (Mod1 and Mod2) over estimate the D_{POA} simulated, mostly at over $600 \text{ W/m}^2 G_{POA}$.

On the other hand, the second plot shows a cloudy-like day where DPOA simulated data and results from Mod1, Mod2A and Mod2B can be observed. In this case, both models (Mod1 and Mod2) show similar performance, with slight under-estimation at the beginning and the end of the day.

In both plots the blue dashed line represents the G_{POA} simulated from SolarGIS, the orange dashed line represents the D_{POA} simulated from SolarGIS, the green dashed line represents the D_{POA} calculated with Mod1, the red dashed line (in this example follows the Mod2B results) represents the D_{POA} calculated with Mod2A and the purple dashed line represents the D_{POA} calculated with Mod2B.

4 CONCLUSIONS AND FUTURE WORK

In this work, two models for POA irradiance separation have been evaluated. Mod1 has a straightforward equation to calculate the diffuse index in POA while Mod2 has two different approaches and it is a piece-wise like function defined by the clearness index in POA value.

In general terms, for 17 different datasets containing SolarGIS data and measured data, Mod1 has shown a better performance than Mod2A, with 3 RSMD percentage points, 5 nRSMD normalized percentage points and $0.05 R^2$, and also than Mod2B, with 3 RSMD percentage points, 5 nRSMD normalized percentage points and $0.05 R^2$.

In future work, on the one hand, it is important to validate the models against high quality measurements of D_{POA} at different sides. On the other hand, the sensitivity of the model accuracy to the overall modeling of shading losses and energy yields has to be evaluated.

Freiburg, 2015, pp. 1–10.

5 ACKNOWLEDGMENT

The authors acknowledge the financial support by the Federal Ministry for Economic Affairs and Energy of Germany (BMWi) in the project ALPRO (project number 0324054A).

6 REFERENCES

- [1] D.G. Erbs, S.A. Klein, J.A. Duffie, Estimation of the diffuse radiation fraction for hourly, daily and monthly-average global radiation, *Solar Energy* 28 (1982) 293–302.
- [2] R. Perez, P. Ineichen, E.L. Maxwell, R.D. Seals, A. Zelenka, Dynamic global-to-direct irradiance conversion models, *ASHRAE Transactions* 98 (1992).
- [3] C.A. Gueymard, J.A. Ruiz-Arias, Extensive worldwide validation and climate sensitivity analysis of direct irradiance predictions from 1-min global irradiance, *Solar Energy* 128 (2016) 1–30.
- [4] N.A. Engerer, Minute resolution estimates of the diffuse fraction of global irradiance for southeastern Australia, *Solar Energy* 116 (2015) 215–237.
- [5] D.E. Guzman Razo, B. Müller, C. Wittwer (Eds.), Ein Modellansatz zur Bestimmung von Direkt- und Diffusanteil der Einstrahlung auf die PV-Modulebene, 34. PV-Symposium Bad Staffelstein, 2019.
- [6] S. Halilovic, J.M. Bright, W. Herzberg, S. Killinger, An analytical approach for estimating the global horizontal from the global tilted irradiance, *Solar Energy* 188 (2019) 1042–1053.
- [7] B.Y.H. Liu, R.C. Jordan, The interrelationship and characteristic distribution of direct, diffuse and total solar radiation, *Solar Energy* 4 (1960) 1–19.
- [8] R. Perez, P. Ineichen, R. Seals, J. Michalsky, R. Stewart, Modeling daylight availability and irradiance components from direct and global irradiance, *Solar Energy* 44 (1990) 271–289.
- [9] D.T. Reindl, W.A. Beckman, J.A. Duffie, Diffuse fraction correlations, *Solar Energy* 45 (1990) 1–7.
- [10] W. F. Holmgren, C. W. Hansen, M. A. Mikofski, pvlib python: A python package for modeling solar energy systems, *JOSS* 3 (2018) 884.
- [11] C. Gueymard, J.A. Ruiz-Arias, Performance of Separation Models to Predict Direct Irradiance at High Frequency: Validation over Arid Areas, in: E. Frank, P. Papillion (Eds.), Conference proceedings / EuroSun 2014, International Conference on Solar Energy and Buildings, Aix-les-Bains, France, 16-19 September, International Solar Energy Society,